Dual roles of capsular extracellular polymeric substances in the photocatalytic inactivation of *Escherichia coli*: Comparison of *E. coli* BW25113 with its isogenic mutants

Guocheng Huang,[a] Dehua Xia,[a] Taicheng An,[b*], Tsz Wai Ng,[a] Ho Yin Yip,[a] Guiying Li,[b] Huijun Zhao,[c] Po Keung Wong[a*]

School of Life Sciences, The Chinese University of Hong Kong, Shatin, NT, Hong Kong SAR, China [a];

State Key Laboratory of Organic Geochemistry, Guangzhou Institute of Geochemistry, Chinese Academy of Sciences, Guangzhou 510640, China [b];

Centre for Clean Environment and Energy, Griffith School of Environment, Griffith University, Queensland 4222, Australia[c]

***Corresponding Authors:**

Prof. Taicheng An, Tel: +86-20-85291501; Fax: +86-20-85290706; E-mail: antc99@gig.ac.cn

Prof. Po Keung Wong, Tel: +852-39436383; Fax: +852-26035767; E-mail: pkwong@cuhk.edu.hk

The dual roles of capsular extracellular polymeric substances (EPS) in the photocatalytic inactivation of bacteria were demonstrated in a TiO_2-UVA system, by comparing wild type *Escherichia coli* BW25113 and isogenic mutants with up-regulated and down-regulated production of capsular EPS. In a partition system in which direct contact between bacterial cells and TiO_2 particles was inhibited, an increase in EPS was associated with increased bacterial resistance to photocatalytic inactivation. In contrast, when bacterial cells were in direct contact with TiO_2 particles, an increase in capsular EPS decreased cell viability during the photocatalytic treatment. When taken together, these results suggest that although capsular EPS can protect bacterial cells by consuming photo-generated reactive species, it also facilitates photocatalytic inactivation of bacteria by promoting the adhesion of TiO_2 particles to the cell surface. Fluorescence microscopic and scanning electron microscopic analyses further confirmed that high capsular EPS density led to more TiO_2 particles attaching to cells and forming bacteria-TiO_2 aggregates. Calculations of interaction energy, represented by extended Derjaguin-Landau-Verwey-Overbeek (XDLVO) potential, suggested that the presence of capsular EPS enhances the attachment of TiO_2 particles to bacterial cells via acid-base interactions. Consideration of these mechanisms is critical for understanding bacteria-nanoparticle interactions and the photocatalytic inactivation of bacteria.

In recent years, heterogeneous photocatalytic processes that use semiconductor catalysts have emerged as promising microbial disinfection technologies (1-7). Among the various photocatalysts being used, titanium dioxide (TiO_2) has received the greatest interest and has been extensively studied because of its efficiency and perceived environmental safety. Photo-generated reactive charge carriers (e^- and h^+) and reactive oxygen species (ROS: •OH, $•O_2^-$ and H_2O_2) are considered to be the major bactericidal agents (8).

Numerous studies have proven the ability of these reactive species to inactivate various kinds of pathogenic bacteria (9-11). It is widely accepted that the bactericidal effect of TiO_2 is due to the destruction of the cell envelope by ROS generated on the surface of TiO_2 photocatalysts (12). However, considerably less is known about the effect of biological factors on photocatalytic inactivation of bacteria. One biological factor that is likely to influence photocatalytic activity is the presence of capsular bacterial extracellular polymeric substances (EPS), which typically comprise polysaccharides and proteins (13).

Located at or outside the cell surface, EPS have many functions including facilitating bacterial adhesion, providing a protective barrier against environmental stresses, maintaining hydration, and storing nutrients (13). The protective function has been reported to significantly increase bacterial tolerance to antibiotics and

disinfectants both by limiting the transport of biocides and via a direct reaction with the EPS (14, 15). The ROS produced on the surface of TiO_2 act as chemical biocides against bacteria. Therefore, it is reasonable to postulate that capsular EPS can protect cells from oxidative damage.

Previous studies of the effect of EPS on ROS-mediated inactivation of bacteria have reported variable results. Liu et al. compared the inactivation efficiencies of heterotrophic bacteria biofilm with the same bacteria without EPS using nitrogen-doped metal oxide a photocatalyst (16). They observed higher inactivation efficiency when the soluble EPS were removed by centrifugation, supporting the hypothesis that EPS act as a protective barrier against ROS-mediated damage to cells. However, a systematic study by Gong et al. showed that the amount of EPS had no observable effect on the susceptibility of four *Escherichia coli* (*E. coli*) isolates to •OH generated via nitrate photolysis (17). The discrepancy between these results may be attributable to differences in the amount of EPS. The EPS levels within the heterotrophic biofilm, which can be up to 90% of the organic carbon (18), are much higher than those in the capsule of *E. coli* isolates. Nonetheless, it must be noted that other factors such as light source, ROS source (photocatalysis or photosensitization) and EPS extraction methods were also different in these studies and may account for the discrepant results. To clarify the role of EPS in the photocatalytic inactivation of

bacteria, it is necessary to conduct a direct comparison by using the same model photocatalysts as well as the same bacterium with differing levels of capsular EPS.

The presence of capsular EPS has a significant effect on the characteristics of the cell surface and may also determine the adhesion of TiO_2 and subsequently influence photocatalytic inactivation efficiency. As photo-generated ROS are highly reactive and short-lived (19, 20), the transport of bacterial cells to the site of surface-generated ROS remains a rate-limiting step in photocatalytic bacterial inactivation (3). Many studies have shown that close contact between bacterial cells and TiO_2 particles increases the extent of oxidative damage (21-23). The production of capsular EPS has been shown to facilitate bacterial adhesion onto various substrates, and the bacterial attachment is well explained and predicted by the extended XDLVO theory (24). Nevertheless, the role of capsular EPS in the physicochemical interactions between bacterial cell and TiO_2 particles during the photocatalytic inactivation of bacteria has yet to be explored (25). A deeper understanding of how capsular EPS affects the adhesion of TiO_2 to bacterial cells would allow us to better interpret the underlying photocatalytic inactivation mechanism, and thereby predict the antibacterial activity of photocatalysts.

The primary objective of this study was to better understand the roles of capsular EPS during the photocatalytic inactivation of bacteria, using wild type *E. coli*

Applied and Environmental Microbiology

99 BW25113 and two isogenic mutants with reduced and increased capsular EPS
100 secretion in a TiO_2-UVA system. The photocatalytic inactivation of the wild type
101 (parental strain) and mutant bacterial cells was compared under the same conditions
102 with and without direct contact with TiO_2 particles (a non-partition system and
103 partition system, respectively). The ROS involved in the inactivation mechanisms
104 were investigated using a scavenger addition study, FT-IR and fluorescence
105 microscopic analyses. Additionally, the interaction of TiO_2 with bacterial cells in the
106 dark was investigated by fluorescence microscopy and scanning electron microscopy
107 and XDLVO potential analysis was used to interpret the results.

108 ## MATERIALS AND METHODS

109 **Bacterial strains and culture.** *E. coli* strain BW25113 (wild type), and its
110 single-gene deletion mutants JW2034 (*cpsB* gene deletion) and JW5917 (*rcsC* gene
111 deletion) were obtained from the Coli Genetic Stock Center (CGSC, Department of
112 Biology, Yale University). All of the strains belong to the Keio collections (Table S1)
113 (26), which are widely used for the study of genetic effects in photocatalytic bacterial
114 inactivation (27-29). Detailed comparisons between the bacterial strains and the wild
115 type can be found in Table S1. The two capsular EPS mutants, *E. coli* JW2034 and *E.*
116 *coli* JW5917, were expected to have different amounts of colanic acid, which is a
117 capsular exopolysaccharide found in many enterobacteria (30, 31). Colanic acid

contents were expressed as glucose content according to the phenol-sulfuric acid method with an average of three replicates. The bacterial cells were cultured in Nutrient Broth 'E' (Lab M, Lancashire, UK; ingredients: 1 g/L beef extract, 2 g/L yeast extract, 5 g/L peptone and 5 g/L sodium chloride) at 37 °C and agitated at 200 rpm for 16 h. The cultures were then harvested according to the method used in previous studies (32, 33).

Photocatalytic inactivation. The photocatalytic inactivation was carried out in a photocatalytic reactor and TiO_2 (P25, Degussa Corporation, Germany) was used for all of the experiments. A UV tube (λ_{max} = 365 nm, 15 W, 60 Hz, Cole-Parmer, USA) was chosen as a light source, and the light intensity was measured with a UVX digital radiometer (UVP, Upland, CA, USA), and fixed at 0.18 mW/cm^2. In the non-partition system (Fig. 1a), the reaction mixture consisted of 2×10^7 cfu (colony forming unit)/mL and 100 mg/L TiO_2 in 50 mL saline (0.9% NaCl) solution. In the partition system (Fig. 1b), a semipermeable membrane compartment with 20 mL bacterial cells in saline solution (2×10^7 cfu/mL) was immersed in 50 mL saline with 100 mg/L TiO_2. A magnetic stirrer was used to ensure suitable suspension in the mixture. At different time intervals, 1 mL aliquots of the cell suspension were collected and serially diluted with sterilized saline solution; 0.1 mL of the diluted sample was then immediately spread on Nutrient Agar (Lab M, Lancashire, UK) plates. The ingredients of the

prepared plates were 5 g/L peptone, 3 g/L beef extract, 8 g/L sodium chloride with 1.2 g/L agar. Subsequently, the agar plates were incubated at 37 °C for 24 h to determine the number of surviving cells (in cfu). For comparison, dark (photocatalyst and bacterial cells without light), light (bacterial cells and light without photocatalyst) and negative controls (bacterial cells alone) were also included in the study. All glassware used in the experiments was washed with deionized (DI) water, and then autoclaved at 121 °C for 20 min to ensure sterility. All treatments and control experiments were performed in triplicate.

EPS purification and quantification. The capsular EPS were extracted, purified, and quantified according to a previous study with some modification (34). In brief, cells were washed twice in saline solution by centrifugation (5000 rpm, 10 min, 4^{o}C) to remove any traces of the media. The washed cells were resuspended in saline solution and incubated for 1 h in a 30°C incubator. The supernatant was recentrifuged at 13000 rpm at 4°C for 60 min to remove residual cells. The resulting supernatant (containing the EPS) was precipitated with 1:3 volume cold ethanol and held at -20°C overnight. The precipitate was separated by centrifugation at 13000 rpm at 4°C for 30 min. The pellet was redissolved in ultrapure water, dialyzed (molecular weight cut-off of 3500 Da, Spectrum Laboratories, Inc.) for 48 h against ultrapure water and then freeze-dried. The EPS were redissolved and then analyzed using the phenol-sulfuric

156 acid method with glucose as standard.

157 **Bacterial cell characterization.** The zeta potentials of TiO_2 P25 and bacterial
158 cells in saline solution (*ca.* 154 mM NaCl) were measured with a ZetaPlus system
159 (Brookhaven Instruments Co., New York) at 25 °C.

160 Fourier Transform Infrared Spectroscopy (FT-IR) was used to probe the chemical
161 and structural composition of the bacteria and assess changes induced by the
162 photocatalytic treatment. Bacterial cells were stained with a LIVE/DEAD BacLight^{TM}
163 Bacterial Viability Kit (L7012, Molecular Probes, Inc., Eugene, OR) and cell
164 membrane integrity was monitored with a fluorescence microscope and a microplate
165 reader, following the procedure recommended by the manufacturer. The live bacterial
166 cells with intact membranes were stained green; dead bacterial cells with damaged
167 membranes were stained red. Scanning electron microscopy (SEM) was used to
168 observe the interaction of bacterial cells and TiO_2. Detailed descriptions of these
169 procedures are described in the supporting text.

170 **Scavenger study.** Scavenger experiments were conducted by adding various
171 scavengers to the non-partition system. Isopropanol was used to remove •OH
172 diffusing into the solution, sodium oxalate ($Na_2C_2O_4$) to remove h^+,
173 4-hydroxy-2,2,6,6-tetramethylpiperidinyloxy (TEMPOL) to remove $\bullet O^{2-}$, Cr(VI) to
174 remove e^-, and Fe(II)-EDTA to remove H_2O_2 (35). The concentration of the scavenger

added was optimized according to our previous studies (32, 35) (0.5 mM for sodium oxalate, 5 mM for isopropanol, 0.05 mM for Cr(VI), 2 mM for TEMPOL and 0.1 mM for Fe(II)-EDTA).

XDLVO interaction between bacterial cells and TiO_2 nanoparticles. The extended Derjaguin-Landau-Verwey-Overbeek (XDLVO) theory was used to model the interaction between bacterial cells and TiO_2 nanoparticles. This theory considers the total energy of adhesion to be the sum of the electrostatic double layer (EL) interaction energy, Lifshiitz-van der Waals (LW) interaction energy, and the Lewis acid-base (AB) (i.e., hydrophobic) interaction energy (36-39). Details of the procedures are described in the supporting text.

Statistical analysis. Results are expressed as mean ± standard deviation. For all of the inactivation experiments, the differences between the survival of cells of wild type and mutant strains at different exposure times were determined using repeated-measures ANOVA. In addition, the differences between the measured parameters were determined using one-way ANOVA. All statistical analyses were carried out using SPSS 16.0 statistical software (IBM Corporation, Somers, NY), and $p < 0.01$ was considered to be statistically significant.

RESULTS AND DISCUSSION

Characterization of bacteria. The *E. coli* BW25113 wild type and isogenic

194 capsular EPS mutants *cpsB*$^-$ and *rcsC*$^-$ were used to investigate the roles of capsular
195 EPS in the photocatalytic inactivation of bacteria. Fig. 1c shows the capsular EPS
196 content of three bacterial strains. *E. coli* JW2034 has a knockout mutation in the *cpsB*
197 gene, which is involved in colanic acid biosynthesis, thus colanic acid production is
198 reduced compared with wild type ($p < 0.01$). The *cpsB*$^-$ mutant is still able to produce
199 some capsular EPS, however, probably due to the complementation of other *cps* genes
200 (40). In contrast, *E. coli* JW5917 has a mutation in the regulatory gene, *rcsC*, so
201 colanic acid production is enhanced compared with the wild type ($p < 0.01$).

202 FT-IR was used to probe the chemical and structural aspects of the total biomass
203 of bacteria. The specific functionality and band assignments were based on previous
204 reports for bacteria and model organic compounds (41-43). Information on the
205 composition and functionality of the cell constituents was extracted from the regions
206 3000-2600 cm^{-1} and 1850-950 cm^{-1} and spectra were normalized to allow the
207 differences in the bands to be compared on the same scale (Fig. S1). The spectra of
208 each particular region were divided by the value of the spectral integral of that region.
209 Band assignments were based on previous reports for bacteria (41, 42). Several
210 common features were observed in all FT-IR spectra, demonstrating the presence of
211 polysaccharides, proteins, fatty acids and phospholipids in these three strains. The
212 strains also shared homologous spectral morphology, indicating that there are no

significant differences in the chemical composition of the wild type and its mutants. Closer observation of Fig. S1 reveals that the three strains possessed different normalized intensity in the region from 950 to 1200 cm^{-1}, corresponding to the C-O, C-O-O, and C-O-P stretching vibrations of polysaccharides (41), with the intensity following the order: *rcsC*⁻ mutant > wild type > *cpsB*⁻ mutant. Given the genetic differences of these three strains, the variation of normalized absorbance in polysaccharide bands is attributed to different capsular EPS production capabilities. This observation supports the rationale of using *E. coli* BW25113 and its isogenic mutants to investigate the role of capsular EPS in photocatalytic inactivation.

Effects of capsular EPS on photocatalytic inactivation. Photocatalytic inactivation in the non-partition system is shown in Fig. 1a. The TiO_2 dose was 100 mg/L, which was optimized in our previous study (27). The dark, light and negative controls showed no obvious reduction in cell population (Figs. S2 and S3), suggesting that TiO_2 or UVA alone did not have a bactericidal affect. When the three strains were subjected to photocatalytic inactivation by exposure to UVA for 60 min in the presence of TiO_2, the susceptibility of the two mutants was different from the wild type ($p < 0.01$). The wild type and overproducing strains were more sensitive to photocatalytic inactivation: the *rcsC*⁻ mutant (exhibiting increased colanic acid production) experienced the greatest decline, followed by the wild type and then the

232 *cpsB*$^-$ mutant (exhibiting decreased colanic acid production). The different
233 susceptibilities of the bacterial strains were probably due to different surface
234 characteristics (e.g. the amount of capsular EPS), which will be further discussed
235 below.

236 To further investigate the significance of capsular EPS when there is no direct
237 contact between TiO_2 and bacterial cells, the inactivation experiment was also
238 conducted in a partition system (Fig. 2b). In the partition system (Fig. 1b), bacterial
239 cells and TiO_2 were separated by a semipermeable membrane, which prohibited direct
240 contact between cells and TiO_2 (35). Significantly lower inactivation efficiencies were
241 observed for all three strains compared with the non-partition system, indicating that
242 direct contact between TiO_2 and bacterial cells is required for effective inactivation.
243 Interestingly, the susceptibility of the bacterial strains to photocatalytic inactivation
244 exhibited a reverse trend, with *cpsB*$^-$ mutant > BW25113 wild type > *rcsC*$^-$ mutant,
245 suggesting that capsular EPS can protect the cell from attack by diffusible ROS when
246 the cells do not make direct contact with TiO_2 nanoparticles. To further explore the
247 protective role of capsular EPS, inactivation efficiencies were compared under only
248 H_2O_2 (10 mM) and •OH, generated by the Fenton reaction (10 mM H_2O_2 and 0.2 mM
249 Fe_2SO_4) (Fig. S4). As expected, the sensitivity of the strains followed the order
250 *cpsB*$^-$ > BW25113 wild type > *rcsC*$^-$. Much higher inactivation efficiencies were

observed from the Fenton reaction than H_2O_2 alone, suggesting that •OH may play a more important role in the inactivation of bacterial cells than H_2O_2 in this system. These results support the hypothesis that the presence of capsular EPS provides some degree of protection to bacterial cells in the presence of these ROS.

The photocatalytic inactivation mechanism. Scavenger studies have been used to systematically investigate the effect of various reactive species that are responsible for photocatalytic inactivation. To better understand the influence of capsular EPS on the photocatalytic inactivation process, the scavenger studies were applied to the *E. coli* BW25113 wild type and the two mutants (Fig. 3). For Cr(VI) (e^- scavenger), TEMPOL ($•O_2^-$ scavenger), isopropanol (diffusing •OH scavenger) and Fe(II)-EDTA (H_2O_2 scavenger), the degree of bacterial inactivation was the same for all three strains. When sodium oxalate (an h^+ scavenger) was added, the cell density of all strains only decreased to ~5 log, which suggests h^+ plays a moderate role in bacterial inactivation. Interestingly, the three strains exhibited different susceptibilities toward photocatalytic inactivation with the addition of oxalate. In the first 10 min, the cell populations of both the wild type and *rcsC*$^-$ mutant only decreased by less than 0.5 log, while the *cpsB*$^-$ mutant experienced a sharp decrease. This suggests that h^+ plays a more important role in the inactivation of the capsular EPS producing strain and overproducing strain than the strain with no colanic acid production (i.e., less or no

capsular EPS produced). Direct contact of the bacterial cells and TiO_2 is a prerequisite for the bacterial inactivation by h^+ oxidation. Although further confirmation is still necessary, it is possible that the presence of capsular EPS enhances the contact of photocatalysts and bacteria.

FT-IR provides a means to track changes in the cell structure and functionality induced by the photocatalytic treatment. Figs. 4a and 4b show the FT-IR spectra of the wild type at various time intervals. The peaks between 3000-2800 cm^{-1} were attributed to C-H stretching vibrations of $–CH_3$ and $–CH_2$ groups mainly from fatty acid (41, 42). Because the *E. coli* cell membrane is predominantly composed of these bonds, this region can be used to probe the changes in cell membrane integrity. After 3 h, the peaks disappeared, indicating damage to the cell membrane. Most studies have reported that the mechanism for the photocatalytic inactivation of bacteria is cell membrane damage and changes in cell permeability resulting from attack by ROS. In conjunction with alternating fatty-acid bands, the decay and disappearance of the polysaccharide peaks were also observed with increasing reaction time, suggesting the breakdown of polysaccharides with the oxidation of ROS. Polysaccharides are the dominant surface feature of the outer membrane of Gram-negative bacteria and capsular EPS (42, 43). As the ROS produced by TiO_2 are highly reactive, it is reasonable to infer that these molecules are important determinants of photocatalytic

289 inactivation efficiency. The region between 1700 and 1500 cm^{-1} shows the
290 characteristic bands of proteins, where 1700-1600 cm^{-1} is specific to C=O stretching
291 vibrations in the amide-I band and 1600-1500 cm^{-1} is specific to N-H bending
292 vibrations in the amide-II band. These peaks decreased during photocatalytic
293 inactivation, indicating changes to proteins. Unlike the variation observed in the
294 fatty-acid and polysaccharide regions, the amide-I band became dominant after 8 h of
295 photocatalytic treatment, suggesting that proteins are more resistant to photocatalytic
296 peroxidation than fatty acids and polysaccharides.

297 The second derivative spectra in the amide-I region were also obtained to explore
298 the changes in protein secondary structure induced by photocatalytic peroxidation
299 (43). Table S3 summarizes the secondary structures present in *E. coli.* As seen in Fig.
300 4c, the untreated bacteria cell largely consisted of β-sheets, α-helices and aggregated
301 strands, with 3-turn helices as a minor feature. A significant breakdown in the protein
302 secondary structure was observed after 1 h. It is significant that cell membranes
303 consist of a lipid bilayer with embedded proteins; in *E. coli*, the cell membrane
304 contains more proteins than lipids (44). These proteins are held in the membrane as a
305 result of hydrophobic interactions between the membrane lipids and the proteins. The
306 secondary structural conformation of proteins (either in α or β), with their
307 hydrophobic side chains oriented toward the outside of the molecule where they

interact with membrane lipids, is a prerequisite of an intact biological membrane (44). In our study, the breakdown of the secondary structure at an early stage of the treatment probably indicates the disruption of the cell membrane architecture.

The LIVE/DEAD BacLight™ Bacterial Viability Kit fluorescent microscopic method was used to reveal changes in cell membrane integrity during the photocatalytic treatment (32, 45). Fig. 5 presents the fluorescence microscopic images of the wild type at different time intervals. Cells that did not undergo photocatalytic treatment were stained green by the nucleic acid binding stain SYTO 9™ (Fig. 5a), which penetrated the bacterial membranes and emitted green light. Propidium iodide only penetrated cells with damaged membranes and emitted red light. After being photocatalytically treated for 5 min, a portion of bacterial cells were stained red (Fig. 5b), indicating a loss of cell membrane integrity (or alteration in membrane permeability). With prolonged irradiation time, more and more red-stained bacterial cells were observed (Figs. 5c and 5d). The fluorescence microscopic observations thus provide strong evidence of bacterial membrane damage from TiO_2-UVA photocatalytic treatment. To quantitatively reveal the cell membrane integrity during the photocatalytic treatment, the fluorescent green to red ratio of the stained cells was obtained using a microplate reader with a standard curve (Fig. S5). All bacterial cells lost their cell membrane integrity with prolonged photocatalytic treatment.

Susceptibility ($p < 0.01$) followed the order *rcsC*$^-$ > wild type > *cpsB*$^-$, which is consistent with the results of the plates count. However, the fluorescent green to red ratio dropped to zero after 60 min for all three strains, whereas viable cells were still observed for the *cpsB*$^-$ mutant and wild type using the plates count method. This discrepancy is probably due to the low detection limit (6 log) of the microplate scale fluorochrome assay with the LIVE/DEAD BacLight^{TM} Bacterial Viability Kit (46).

These findings indicate that ROS produced by TiO_2 act as nonselective oxidants to cell surface biomolecules, including lipids, polysaccharides and protein. Clearly, the cell membrane is essential to the survival of bacterial cells. Damage of the cell membrane by ROS has been reported to be the fundamental mechanism of photocatalytic inactivation of bacteria (21, 47, 48). Thus, it is not surprising that capsular EPS could decrease inactivation efficiency by competing with the cell membrane for available ROS. Among the ROS produced, •OH and $•O_2^-$ are short-lived and function at very close vicinity of the TiO_2 surface. H_2O_2 is much longer-lived, but much less detrimental (49). It is also possible that direct attack of the cell membrane by e^- or h^+ could cause lethal damage to the cell. In this instance, the close contact between the photocatalyst particles and the bacteria is the key to obtaining high photocatalytic inactivation efficiencies. In the present study, the presence of capsular EPS enhanced the photocatalytic inactivation of bacteria in a

346 non-partition system using TiO_2-UVA. It is very likely that capsular EPS enhances the
347 adhesion of TiO_2 to the surface of bacterial cells, thereby leading to photocatalytic
348 inactivation of the bacteria. This effect appears to outweigh the protective role of the
349 EPS.

350 **Capsular EPS-mediated adhesion of TiO_2 to bacteria.** Fluorescence
351 microscopic and SEM analyses were used to investigate the interaction of TiO_2 with
352 the three strains in the dark and to determine how capsular EPS play a role in this
353 interaction. In the absence of any TiO_2 particles, all of the live *E. coli* cells were
354 homogeneously suspended and did not agglomerate (Fig. S6). After 30 min contact
355 with TiO_2 in the dark, cells of the wild type and the *rcsC*$^-$ mutant (EPS overproducing
356 strain) started to form aggregates (Figs. 6a and 6c), whereas cell aggregation was not
357 observed for the *cpsB*$^-$ mutant (Fig. 6b). Direct observation by SEM revealed more
358 TiO_2 particles loaded on the cell surface of the wild type and *rcsC*$^-$ mutant (Figs. 6d
359 and 6f). For the *cpsB*$^-$ mutant, most of the TiO_2 particles were seen on the slip beside
360 the cells (Fig. 6e). The energy dispersive X-Ray (EDX) spectra (Fig. S7) confirmed
361 this observation. These results suggest that capsular EPS play an important role in the
362 interaction of the bacterial cells with TiO_2 particles, which is certainly involved in the
363 inactivation mechanisms of the photocatalytic process.

364 To understand the role of capsular EPS in adhesion interactions the XDLVO

365 approach was used to evaluate the physicochemical forces for contact between TiO_2
366 and the bacterial cells. It was assumed for calculation purposes that the bacterial cells
367 were spherical, with a radius around 0.5 μm based on SEM images. Agglomerates of
368 TiO_2 were assumed to be monodispersed spheres with radii 200 nm. The interactions
369 between the bacterial cells and TiO_2 did not appear to be greatly influenced by radius
370 size as the calculated EL, LW, and AB interaction energies were in the same order of
371 magnitude.

372 The zeta potentials of the bacterial cells and TiO_2 were also used to represent
373 surface potentials (Fig. S8) (38). Zeta potential measurements reveal that these three
374 strains are all negatively charged, whereas TiO_2 was positively charged at the test pH
375 (6.5) of the photocatalytic treatment, indicating an attractive EL interaction between
376 the bacterial cells and TiO_2 nanoparticles. Average contact angles were measured for
377 three probe liquids on four lawns (TiO_2, wild type, *cpsB*$^-$ mutant and *rcsC*$^-$ mutant);
378 these are listed in Table S4. The values of γ^{LW}, γ^+, γ^-, A and $\Delta G_{d_0}^{AB}$ for the
379 three strains and TiO_2 were calculated using the equation in the supporting text and
380 shown in Table 1. The Hamaker constant A of the bacteria-water-TiO_2 system for
381 wild type, *cpsB*$^-$ mutant and *rcsC*$^-$ mutant was calculated as -0.512×10^{-21}, $-0.979 \times$
382 10^{-21} and 0.177×10^{-21} J respectively, suggesting a repulsive LW interaction between
383 TiO_2 nanoparticles and the capsular EPS overproducing strain, while an attractive LW

384 interaction with TiO_2 was obtained for the wild type and non-capsular EPS strain. The
385 calculated values $\Delta G_{d_0}^{AB}$ in bacteria-water-TiO_2 for wild type, *cpsB*⁻ mutant and *rcsC*⁻
386 mutant were -2.25, 1.81 and -3.60 mJ/m^2, respectively, indicating that the presence of
387 capsular EPS favored an attractive interaction between TiO_2 nanoparticles and
388 bacterial cells while the absence of capsular EPS resulted in a repulsive AB
389 interaction.

390 The total XDLVO interaction profiles reflect the sum of EL, LW and AB
391 interaction. The characteristic XDLVO interaction profiles between the three strains
392 and TiO_2 as a function of distance are shown in Fig. 7a. Both the wild type and *rcsC*⁻
393 mutant experienced attraction with TiO_2 from 4 nm, and the value of total energy
394 increased with decreasing distance until they reached the primary minimum. However,
395 the total energy for the *cpsB*⁻ mutant interaction with TiO_2 was always positive below
396 4 nm. According to this energy profile adhesion would not occur for the *cpsB*⁻ mutant.
397 These results accord with the results from the fluorescence microscopic and SEM
398 analyses, which suggest that the presence of capsular EPS facilitated the adhesion of
399 TiO_2 to bacterial cells, as well as their aggregation. Based on the different approaches
400 of TiO_2 toward the cell, the order of the inactivation efficiencies in the non-partition
401 system can be qualitatively explained by the XDLVO theory. The magnitude of the
402 AB interaction energy was generally higher than those of the EL and LW (Figs. 7b, 7c

and 7d). Previous studies have shown that nanoparticles attached on surfaces increases with the presence of biofilm EPS, in a way that cannot be well predicted by the traditional Derjaguin-Landau-Verwey-Overbeek (DLVO) theory (50-52). The results of this study suggest that the interactions between bacteria and nanoparticles may be largely governed by the AB (hydrophobic) interaction, which coincides well with the XDLVO theory in which a hydrophobic interaction energy is added to the DLVO theory. Though there are many studies stating interactions between nanoparticles and EPS, few have focused on how capsular EPS levels affect the interaction and how EPS-nanoparticle interactions affect the viability of bacteria. As we have shown, the presence of capsular EPS influenced the physicochemical properties of the surface of bacterial cells and resulted in a strong attractive AB interaction, which consequently improved photocatalytic inactivation efficiency.

CONCLUSION

Overall, the findings obtained from this study suggest that capsular EPS play a dual role in the photocatalytic inactivation of bacteria: (i) the presence of capsular EPS can protect the bacterial cell by consuming photo-generated reactive species; and (ii) capsular EPS promotes the adhesion of TiO_2 particles to the cell surface and subsequently enhances photocatalytic efficiency. These results not only broaden the

limited literature concerning the effect of capsular EPS on the photocatalytic inactivation of bacteria, but they also have important implications for the transport and fate of TiO_2 nanoparticles in aquatic environments.

From a practical point of view, capsular EPS, as a mediator of bacterial cell-TiO_2 aggregate formation and a protective barrier for bacterial cells has to be taken into account in the design and operation of photocatalytic disinfection technology. The presence of capsular EPS can enhance photocatalytic inactivation efficiencies due to the formation of bacteria-TiO_2 aggregates. More generally, the applicability of XDLVO theory to bacteria-nanoparticle interactions demonstrated by this work has important implications not only for modeling and predicting photocatalytic inactivation in natural and engineered systems, but also for the further investigations of nanomaterial for various disciplines where bacteria-nanoparticle interactions are important preconditions. For instance, the investigations of (i) contact between metal-reducing bacteria and metal-bearing minerals that are required for dissimilatory growth (53); (ii) hybrid systems that combine the catalytic and synthetic power of bacteria with the optoelectronic capabilities of nanomaterials (54); and (iii) nanotoxicity studies (55). Our results highlight the critical role of capsular EPS in bacteria-nanoparticle interactions and this should be taken into account in future bacteria-nanoparticle studies.

Applied and Environmental Microbiology

441 To the best of our knowledge, studies using single-gene knockout mutants to
442 investigate the mechanism of photocatalytic inactivation are still very limited.
443 Nevertheless, the findings of this study suggest that comparing different mutants with
444 the parental strain is an important way to better understand the mechanism of
445 photocatalytic inactivation of bacteria.

446 **ACKNOWLEDGMENTS**

447 The project was supported by a research grant (GRF476811) of the Research Grant
448 Council, Hong Kong SAR Government and CAS/SAFEA International Partnership
449 Program for Creative Research Teams to P.K. Wong, and the research grant
450 (41373102 and 21077104) of National Science Foundation of China to T.C. An and
451 G.Y. Li.

452

REFERRENCES

1. **Shannon MA, Bohn PW, Elimelech M, Georgiadis JG, Marinas BJ, Mayes AM.** 2008. Science and technology for water purification in the coming decades. Nature **452:**301-310. http://dx.doi.org/10.1038/nature06599.
2. **Zhang LS, Wong KH, Chen ZG, Yu JC, Zhao JC, Hu C, Chan CY, Wong PK.** 2009. AgBr-Ag-Bi_2WO_6 nanojunction system: A novel and efficient photocatalyst with double visible-light active components. Appl. Catal. A-Gen. **363:**221-229. http://dx.doi.org/10.1016/j.apcata.2009.05.028.
3. **Chong MN, Jin B, Chow CWK, Saint C.** 2010. Recent developments in photocatalytic water treatment technology: A review. Water Res. **44:**2997-3027. http://dx.doi.org/10.1016/j.watres.2010.02.039.
4. **Zhang LS, Wong KH, Yip HY, Hu C, Yu JC, Chan CY, Wong PK.** 2010. Effective photocatalytic disinfection of E. coli K-12 using AgBr-Ag-Bi_2WO_6 nanojunction system irradiated by visible Light: The role of diffusing hydroxyl radicals. Environ. Sci. Technol. **44:**1392-1398. http://dx.doi.org/10.1021/Es903087w.
5. **Chen YM, Lu AH, Li Y, Zhang LS, Yip HY, Zhao HJ, An TC, Wong PK.** 2011. Naturally occurring sphalerite as a novel cost-effective photocatalyst for bacterial disinfection under visible light. Environ. Sci. Technol. **45:**5689-5695. http://dx.doi.org/10.1021/es200778p.
6. **Zhang LS, Wang HL, Chen ZG, Wong PK, Liu JS.** 2011. Bi_2WO_6 micro/nano-structures: Synthesis, modifications and visible-light-driven photocatalytic applications. Appl. Catal. B-Environ. **106:**1-13. http://dx.doi.org/10.1016/j.apcatb.2011.05.008.
7. **Wong MS, Chu WC, Sun DS, Huang HS, Chen JH, Tsai PJ, Lin NT, Yu MS,**

Hsu SF, Wang SL, Chang HH. 2006. Visible-light-induced bactericidal activity of a nitrogen-doped titanium photocatalyst against human pathogens. Appl. Environ. Microbiol. **72:**6111-6116. http://dx.doi.org/10.1128/Aem.02580-05.

8. **Dalrymple OK, Stefanakos E, Trotz MA, Goswami DY.** 2010. A review of the mechanisms and modeling of photocatalytic disinfection. Appl. Catal. B-Environ. **98:**27-38. http://dx.doi.org/10.1016/j.apcatb.2010.05.001.

9. **Robertson JMC, Robertson PKJ, Lawton LA.** 2005. A comparison of the effectiveness of TiO_2 photocatalysis and UVA photolysis for the destruction of three pathogenic micro-organisms. J. Photochem. Photobiol. A-Chem. **175:**51-56. http://dx.doi.org/10.1016/j.jphotochem.2005.04.033.

10. **Nadtochenko VA, Sarkisov OM, Nikandrov VV, Chubukov PA, Denisov NN.** 2008. Inactivation of pathogenic microorganisms in the photocatalytic process on nanosized TiO_2 crystals. Russ. J. Phys. Chem. B **2:**105-114. http://dx.doi.org/10.1007/s11826-008-1016-0.

11. **Kim TY, Park SS, Kim SJ, Cho SY.** 2011. A study of bactericidal effect and optimization of pathogenic bacteria using TiO_2 photocatalyst. J. Nanosci. Nanotechnol. **11:**1551-1554. http://dx.doi.org/10.1166/jnn.2011.3339.

12. **Pigeot-Remy S, Simonet F, Errazuriz-Cerda E, Lazzaroni JC, Atlan D, Guillard C.** 2011. Photocatalysis and disinfection of water: Identification of potential bacterial targets. Appl. Catal. B-Environ. **104:**390-398. http://dx.doi.org/10.1016/j.apcatb.2011.03.001.

13. **Eboigbodin KE, Biggs CA.** 2008. Characterization of the extracellular polymeric substances produced by *Escherichia coli* using infrared spectroscopic, proteomic, and aggregation studies. Biomacromolecules **9:**686-695. http://dx.doi.org/10.1021/Bm701043c.

14. **Gilbert P, Das J, Foley I.** 1997. Biofilm susceptibility to antimicrobials.

Advances in dental research **11:**160-167. http://dx.doi.org/10.1177/08959374970110010701.

15. **Xue Z, Sendamangalam VR, Gruden CL, Seo Y.** 2012. Multiple roles of extracellular polymeric substances on resistance of biofilm and detached clusters. Environ. Sci. Technol. **46:**13212-13219. http://dx.doi.org/10.1021/es3031165.
16. **Liu Y, Li J, Qiu XF, Burda C.** 2007. Bactericidal activity of nitrogen-doped metal oxide nanocatalysts and the influence of bacterial extracellular polymeric substances (EPS). J. Photochem. Photobiol. A-Chem. **190:**94-100. http://dx.doi.org/10.1016/j.jphotochem.2007.03.017.
17. **Gong AS, Lanzl CA, Cwiertny DM, Walker SL.** 2012. Lack of influence of extracellular polymeric substances (EPS) level on hydroxyl radical mediated disinfection of *Escherichia coli*. Environ. Sci. Technol. **46:**241-249. http://dx.doi.org/10.1021/es202541r.
18. **Nielsen PH, Jahn A, Palmgren R.** 1997. Conceptual model for production and composition of exopolymers in biofilms. Water Sci. Technol. **36:**11-19. http://dx.doi.org/10.1016/S0273-1223(97)00318-1.
19. **Kikuchi Y, Sunada K, Iyoda T, Hashimoto K, Fujishima A.** 1997. Photocatalytic bactericidal effect of TiO_2 thin films: Dynamic view of the active oxygen species responsible for the effect. J. Photochem. Photobiol. A-Chem. **106:**51-56. http://dx.doi.org/10.1016/S1010-6030(97)00038-5.
20. **Mills A, LeHunte S.** 1997. An overview of semiconductor photocatalysis. J. Photochem. Photobiol. A-Chem. **108:**1-35. http://dx.doi.org/10.1016/S1010-6030(97)00118-4.
21. **Gogniat G, Thyssen M, Denis M, Pulgarin C, Dukan S.** 2006. The bactericidal effect of TiO_2 photocatalysis involves adsorption onto catalyst and the loss of membrane integrity. FEMS Microbiol. Lett. **258:**18-24.

http://dx.doi.org/10.1111/j.1574-6968.2006.00190.x.

22. **Cheng CL, Sun DS, Chu WC, Tseng YH, Ho HC, Wang JB, Chung PH, Chen JH, Tsai PJ, Lin NT, Yu MS, Chang HH.** 2009. The effects of the bacterial interaction with visible-light responsive titania photocatalyst on the bactericidal performance. J. Biomed. Sci. **16:**7. http://dx.doi.org/10.1186/1423-0127-16-7.

23. **Pablos C, van Grieken R, Marugan J, Chowdhury I, Walker SL.** 2013. Study of bacterial adhesion onto immobilized TiO_2: Effect on the photocatalytic activity for disinfection applications. Catal. Today **209:**140-146. http://dx.doi.org/10.1016/j.cattod.2012.12.010.

24. **Chia TWR, Nguyen VT, McMeekin T, Fegan N, Dykes GA.** 2011. Stochasticity of bacterial attachment and its predictability by the extended Derjaguin-Landau-Verwey-Overbeek theory. Appl. Environ. Microbiol. **77:**3757-3764. http://dx.doi.org/10.1128/Aem.01415-10.

25. **Thabet S, Simonet F, Lemaire M, Guillard C, Cotton P.** 2014. Impact of photocatalysis on fungal cells: depiction of cellular and molecular effects on Saccharomyces cerevisiae. Appl. Environ. Microbiol. **80:**7527-7535. http://dx.doi.org/10.1128/AEM.02416-14.

26. **Baba T, Ara T, Hasegawa M, Takai Y, Okumura Y, Baba M, Datsenko KA, Tomita M, Wanner BL, Mori H.** 2006. Construction of *Escherichia coli* K-12 in-frame, single-gene knockout mutants: the Keio collection. Molec. Syst. Biol. **2:**2006 0008. http://dx.doi.org/10.1038/msb4100050.

27. **Gao MH, An TC, Li GY, Nie X, Yip HY, Zhao H, Wong PK.** 2012. Genetic studies of the role of fatty acid and coenzyme A in photocatalytic inactivation of *Escherichia coli*. Water Res. **46:**3951-3957. http://dx.doi.org/10.1016/j.watres.2012.05.033.

28. **Nie X, Li GY, Gao MH, Sun HW, Liu XL, Zhao HJ, Wong PK, An TC.** 2014. Comparative study on the photoelectrocatalytic inactivation of *Escherichia coli* K-12 and its mutant *Escherichia coli* BW25113 using TiO_2 nanotubes as a photoanode. Appl. Catal. B-Environ. **147:**562-570. http://dx.doi.org/10.1016/j.apcatb.2013.09.037.

29. **Shi H, Huang G, Xia D, Ng TW, Yip HY, Li G, An T, Zhao H, Wong P.** 2015. Role of in situ resultant H_2O_2 in the Visible-Light-Driven photocatalytic inactivation of E. coli using natural sphalerite: A genetic study. J. Phys. Chem. B **119:**3104-3111. http://dx.doi.org/10.1021/jp511201w.

30. **Ratto M, Verhoef R, Suihko ML, Blanco A, Schols HA, Voragen AGJ, Wilting R, Siika-aho R, Buchert J.** 2006. Colanic acid is an exopolysaccharide common to many enterobacteria isolated from paper-machine slimes. J. Indust. Microbiol. Biotechnol. **33:**359-367. http://dx.doi.org/10.1007/s10295-005-0064-1.

31. **Hanna A, Berg M, Stout V, Razatos A.** 2003. Role of capsular colanic acid in adhesion of uropathogenic Escherichia coli. Appl. Environ. Microbiol. **69:**4474-4481. http://dx.doi.org/10.1128/Aem.69.8.4474-4481.2003.

32. **Xia DH, Ng TW, An TC, Li GY, Li Y, Yip HY, Zhao HJ, Lu AH, Wong PK.** 2013. A recyclable mineral catalyst for visible-light-driven photocatalytic inactivation of bacteria: Natural magnetic sphalerite. Environ. Sci. Technol. **47:**11166-11173. http://dx.doi.org/10.1021/es402170b.

33. **Liu SW, Huang GC, Yu JG, Ng TW, Yip HY, Wongt PK.** 2014. Porous fluorinated SnO_2 hollow nanospheres: Transformative self-assembly and photocatalytic inactivation of bacteria. ACS Appl. Mater. Interf. **6:**2405-2412. http://dx.doi.org/10.1021/Am4047975.

34. **Bergmaier D, Lacroix C, Macedo MG, Champagne CP.** 2001. New method

for exopolysaccharide determination in culture broth using stirred ultrafiltration cells. Appl. Microbiol. Biot. **57:**401-406. http://dx.doi.org/10.1007/s002530100764.

35. **Wang WJ, Yu Y, An TC, Li GY, Yip HY, Yu JC, Wong PK.** 2012. Visible-light-driven photocatalytic inactivation of *E. coli* K-12 by bismuth vanadate nanotubes: Bactericidal performance and mechanism. Environ. Sci. Technol. **46:**4599-4606. http://dx.doi.org/10.1021/es2042977.

36. **Chen G, Strevett KA.** 2003. Microbial surface thermodynamics and interactions in aqueous media. J. Colloid Interf. Sci **261:**283-290. http://dx.doi.org/10.1016/S0021-9797(02)00242-4.

37. **Schwegmann H, Ruppert J, Frimmel FH.** 2013. Influence of the pH-value on the photocatalytic disinfection of bacteria with TiO_2 - Explanation by DLVO and XDLVO theory. Water Res. **47:**1503-1511. http://dx.doi.org/10.1016/j.watres.2012.11.030.

38. **Wang LX, Xu SP, Li J.** 2011. Effects of phosphate on the transport of *Escherichia coli* O157:H7 in saturated quartz sand. Environ. Sci. Technol. **45:**9566-9573. http://dx.doi.org/10.1021/es201132s.

39. **Bayoudh S, Othmane A, Mora L, Ben Ouada H.** 2009. Assessing bacterial adhesion using DLVO and XDLVO theories and the jet impingement technique. Colloid Surface. B **73:**1-9. http://dx.doi.org/10.1016/j.colsurfb.2009.04.030.

40. **Gottesman S, Stout V.** 1991. Regulation of capsular polysaccharide synthesis in *Escherichia coli* K12. Molec. Microbiol. **5:**1599-1606. http://dx.doi.org/10.1111/j.1365-2958.1991.tb01906.x.

41. **Schmitt J, Flemming HC.** 1998. FTIR-spectroscopy in microbial and material analysis. Int. Biodeter. Biodegr **41:**1-11. http://dx.doi.org/10.1016/S0964-8305(98)80002-4.

608 42. **Kiwi J, Nadtochenko V.** 2005. Evidence for the mechanism of photocatalytic
609 degradation of the bacterial wall membrane at the TiO_2 interface by ATR-FTIR
610 and laser kinetic spectroscopy. Langmuir. **21:**4631-4641.
611 http://dx.doi.org/10.1021/La0469831.
612 43. **Badireddy AR, Korpol BR, Chellam S, Gassman PL, Engelhard MH, Lea**
613 **AS, Rosso KM.** 2008. Spectroscopic characterization of extracellular polymeric
614 substances from *Escherichia coli* and *Serratia marcescens*: Suppression using
615 sub-inhibitory concentrations of bismuth thiols. Biomacromolecules **9:**3079-3089.
616 http://dx.doi.org/10.1021/Bm800600p.
617 44. **Nelson DL, Cox MM.** 2004. Lehninger Principles of Biochemistry, Forth
618 Edition. W. H. Freeman, New York.
619 45. **Pigeot-Remy S, Simonet F, Atlan D, Lazzaroni JC, Guillard C.** 2012.
620 Bactericidal efficiency and mode of action: A comparative study of
621 photochemistry and photocatalysis. Water Res. **46:**3208-3218.
622 http://dx.doi.org/10.1016/j.watres.2012.03.019.
623 46. **Alakomi HL, Matto J, Virkajarvi I, Saarela M.** 2005. Application of a
624 microplate scale fluorochrome staining assay for the assessment of viability of
625 probiotic preparations. J. Microbiol. Meth. **62:**25-35.
626 http://dx.doi.org/10.1016/j.mimet.2005.01.005.
627 47. **Liou JW, Gu MH, Chen YK, Chen WY, Chen YC, Tseng YH, Hung YJ,**
628 **Chang HH.** 2011. Visible light responsive photocatalyst induces progressive and
629 apical-terminus preferential damages on *Escherichia coli* surfaces. PLOS One
630 **6:**e19982. http://dx.doi.org/10.1371/journal.pone.0019982.
631 48. **Carre G, Hamon E, Ennahar S, Estner M, Lett MC, Horvatovich P, Gies JP,**
632 **Keller V, Keller N, Andre P.** 2014. TiO_2 photocatalysis damages lipids and
633 proteins in Escherichia coli. Appl. Environ. Microbiol. **80:**2573-2581.

http://dx.doi.org/10.1128/Aem.03995-13.

49. **Imlay JA.** 2003. Pathways of oxidative damage. Annu. Rev. Microbiol. **57:**395-418. http://dx.doi.org/10.1146/annurev.micro.57.030502.090938.

50. **Tong MP, Ding JL, Shen Y, Zhu PT.** 2010. Influence of biofilm on the transport of fullerene (C-60) nanoparticles in porous media. Water Res. **44:**1094-1103. http://dx.doi.org/10.1016/j.watres.2009.09.040.

51. **Lerner RN, Lu QY, Zeng HB, Liu Y.** 2012. The effects of biofilm on the transport of stabilized zerovalent iron nanoparticles in saturated porous media. Water Res. **46:**975-985. http://dx.doi.org/10.1016/j.watres.2011.11.070.

52. **Jiang XJ, Wang XT, Tong MP, Kim H.** 2013. Initial transport and retention behaviors of ZnO nanoparticles in quartz sand porous media coated with Escherichia coli biofilm. Environ. Pollut. **174:**38-49. http://dx.doi.org/10.1016/j.envpol.2012.11.016.

53. **Luef B, Fakra SC, Csencsits R, Wrighton KC, Williams KH, Wilkins MJ, Downing KH, Long PE, Comolli LR, Banfield JF.** 2013. Iron-reducing bacteria accumulate ferric oxyhydroxide nanoparticle aggregates that may support planktonic growth. Isme Journal **7:**338-350. http://dx.doi.org/10.1038/ismej.2012.103.

54. **Sakimoto KK, Liu C, Lim J, Yang P.** 2014. Salt-induced self-assembly of bacteria on nanowire arrays. Nano Lett **14:**5471-5476. http://dx.doi.org/10.1021/nl502946j.

55. **Chen KL, Bothun GD.** 2014. Nanoparticles meet cell membranes: Probing nonspecific interactions. using model membranes. Environ. Sci. Technol. **48:**873-880. http://dx.doi.org/10.1021/Es403864v.

Figure captions

Fig 1. The schematic illustration of photocatalytic inactivation set up, (a) The non-partition system, (b) The partition system; and (c) colanic acid production of the wild type, *cpsB*⁻ mutant and *rcsC*⁻ mutant. Bars represent standard deviations (n=3) and data were statistically significant at $p < 0.001$ calculated by one-way ANOVA.

Fig 2. Comparison of photocatalytic inactivation efficiencies of wild type with its single-gene knock out *cpsB*⁻ mutant and *rcsC*⁻ mutant in (a) non-partition system and (b) partition system. TiO_2 concentration = 100 mg/L, initial cell density = 2×10^7 cfu/mL, light intensity = 0.18 mW/cm^2. Bars represent standard deviations and data were statistically significant at $p < 0.01$ calculated by repeated-measures ANOVA.

Fig 3. Photocatalytic inactivation efficiency of wild type (a) and its single-gene knock out *cpsB*⁻ mutant (b) and *rcsC*⁻ mutant (c), with different scavengers (0.5 mM sodium oxalate, 5 mM isopropanol, 0.05 mM Cr(VI), 2 mM TEMPOL and 0.1 mM Fe(II)-EDTA). Bars represent standard deviations (n=3).

Fig 4. FT-IR spectra of wild type at different irradiation times. Bands in the spectral region of 3000-2650 cm^{-1} (a) and Bands in the spectral region of 1850-950 cm^{-1}(b); and Second derivative spectra in amide I (1700-1600 cm^{-1}) (c).

Fig 5. Fluorescence microscopic images of wild type treated by TiO_2-UVA at (a) 0 min, (b) 5 min, (c) 10 min and (d) 20 min. The scale bars are 20 μm.

682 **Fig 6.** Fluorescence microscopic images of *E. coli* cells after 30 min treatment of
683 contact with TiO_2 nanoparticles in dark: (a) wild type, (b) *cpsB*⁻ mutant and
684 (c) *rcsC*⁻ mutant. The scale bars are 20 μm, and SEM images of *E. coli* cells
685 after 30 min treatment of contact with TiO_2 P25 nanoparticles in dark: (d)
686 wild type, (e) *cpsB*⁻ mutant and (f) *rcsC*⁻ mutant.

687 **Fig 7.** Interaction profiles of (a) wild type, *cpsB*⁻ mutant and *rcsC*⁻ mutant with TiO_2
688 according to XDLVO theory, and the EL (electrostatic double layer), LW
689 (Lifshiitz-van der Waals) and AB (Lewis acid-base) interaction profiles for
690 (b) wild type, (c) *cpsB*⁻ mutant and (d) *rcsC*⁻ mutant, repectively.

691

692

693 **Fig. 1.**

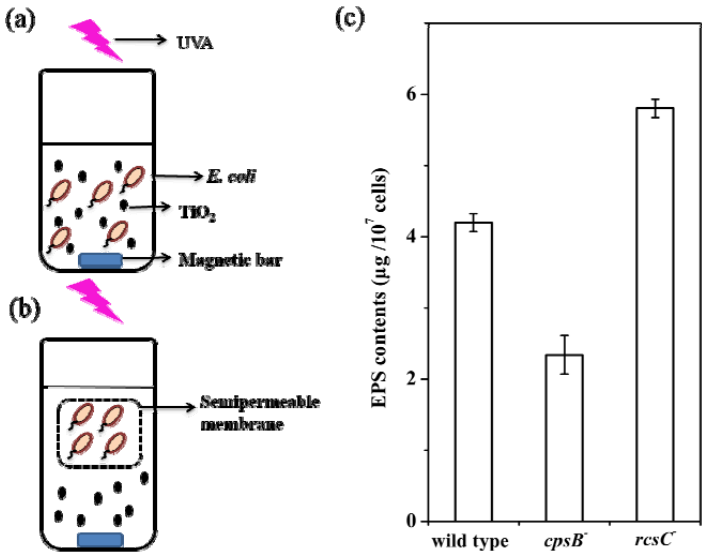

694

695

696 **Fig. 2.**

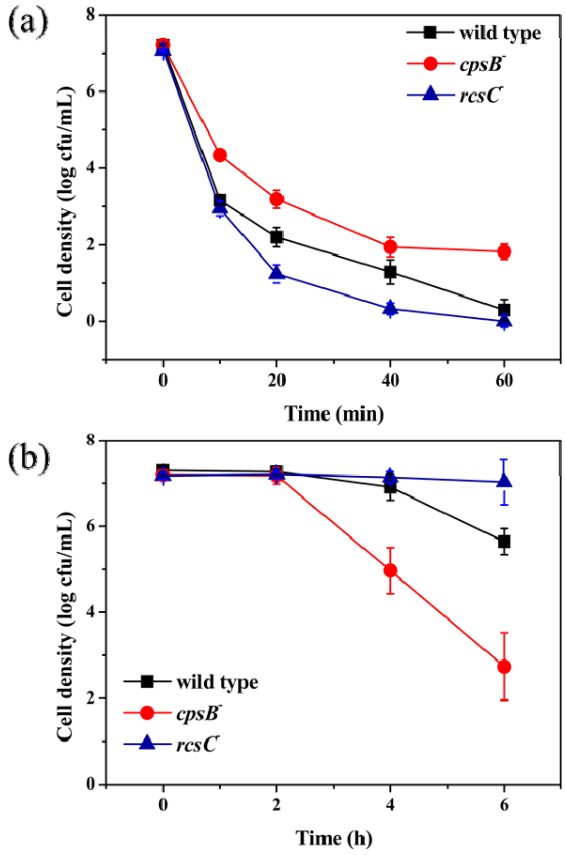

697

698

699 **Fig. 3.**

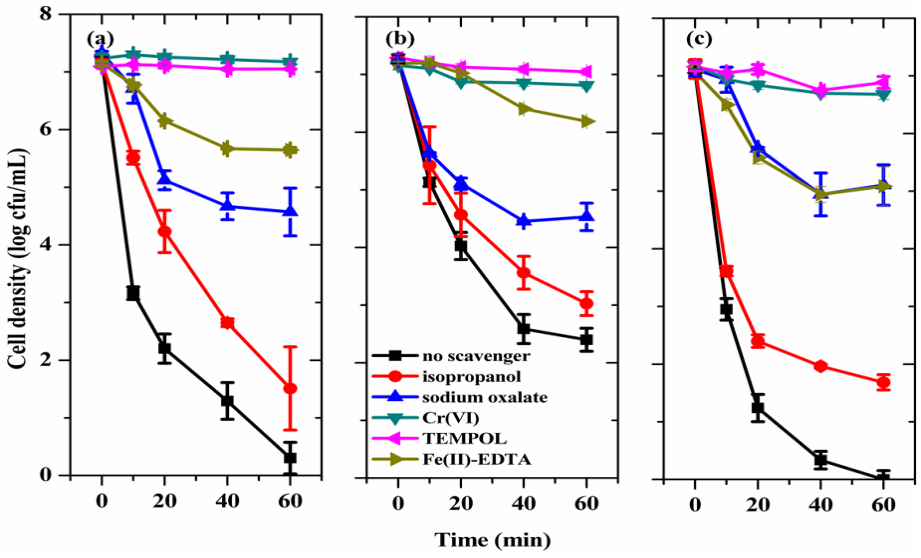

700

701 **Fig. 4.**

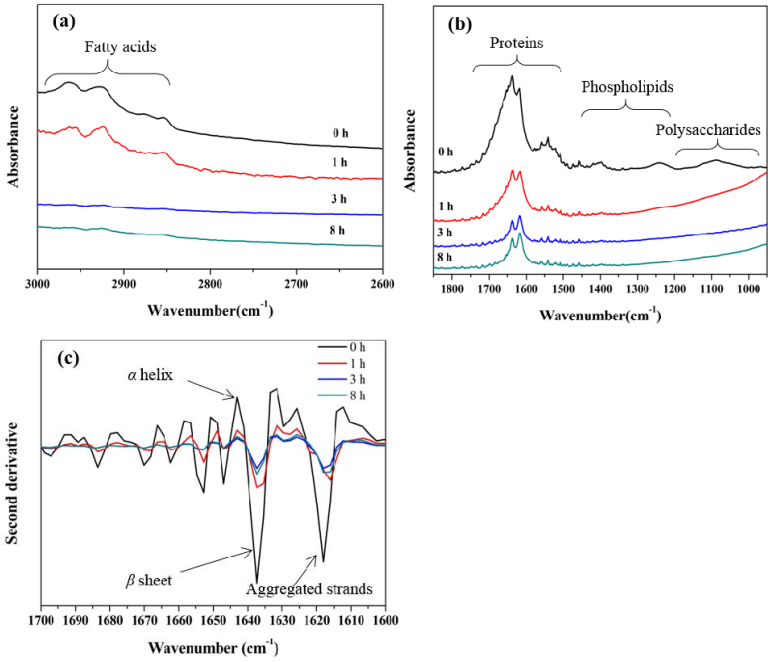

702

703

704 **Fig 5.**

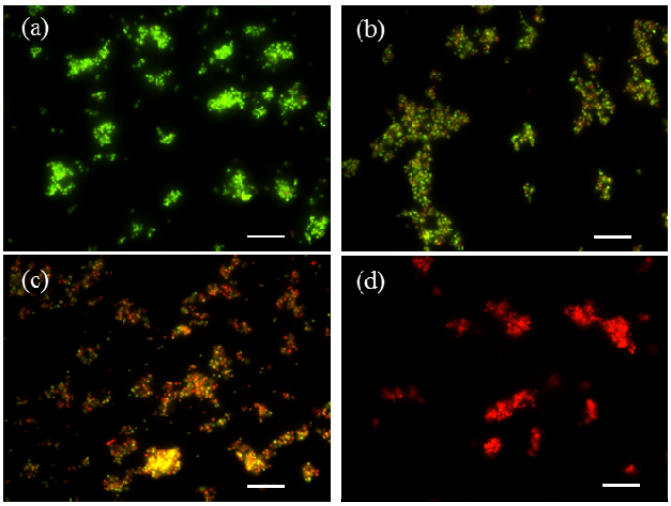

705

706

707 **Fig 6.**

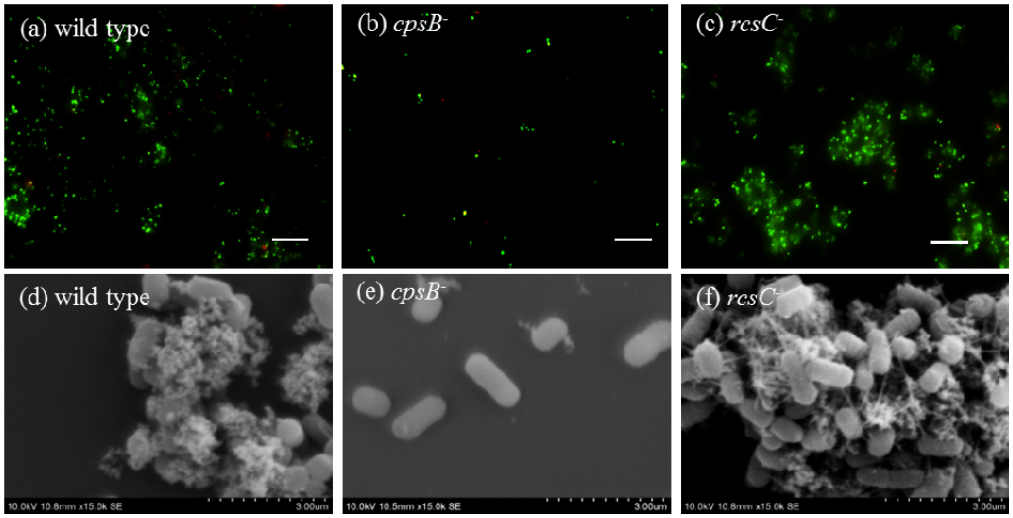

708

709

710 **Fig 7.**

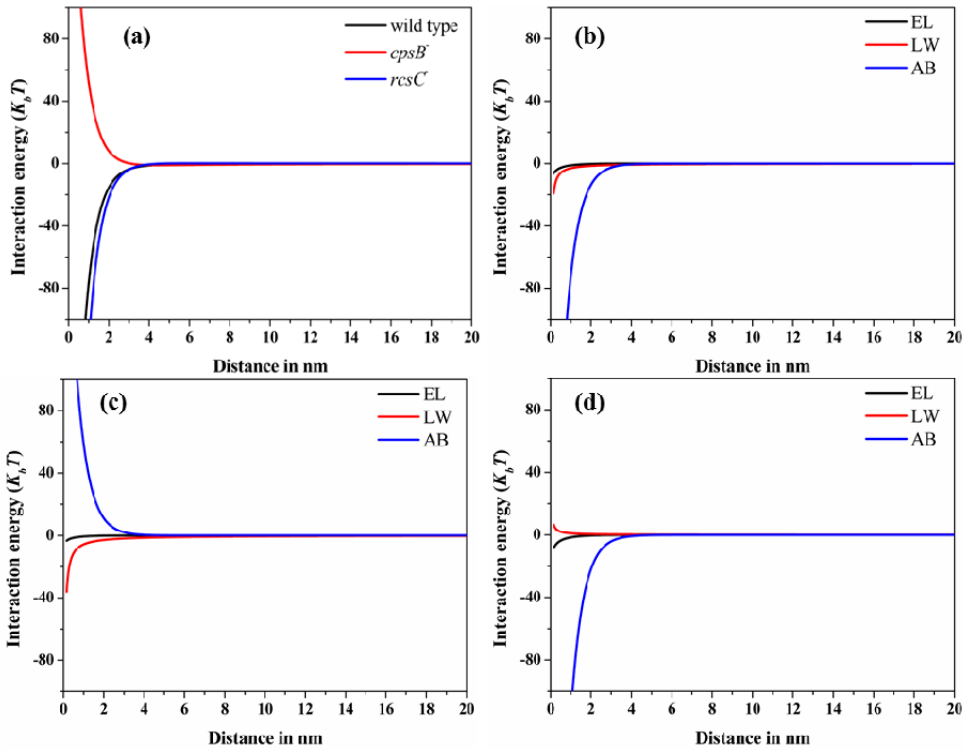

711

712 **Table 1.** Surface energy of TiO_2 and *E. coli* cells in mJ/m^{-2}

	γ_L^{LW}	γ_L^+	γ_L^-	γ_L^{AB}	$\Delta G_{d_0}^{AB}$	A in 10^{-21} J
TiO_2	5.5	47.5	32.2	29.8		
wild type	6.4	43.0	33.1	25.2	-2.3	-0.512
cpsB⁻ mutant	4.8	50.3	30.9	28.4	1.8	-0.979
rcsC⁻ mutant	9.3	42.3	39.7	20.7	-3.6	0.177

713

714

715

Figure 1

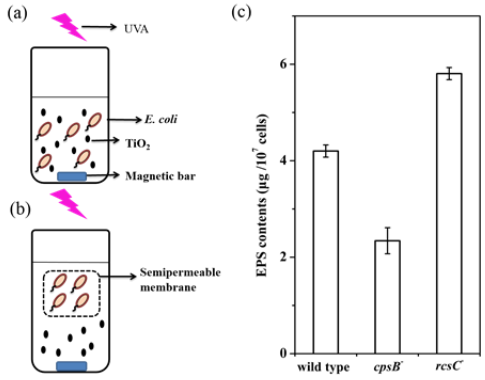

Figure 2

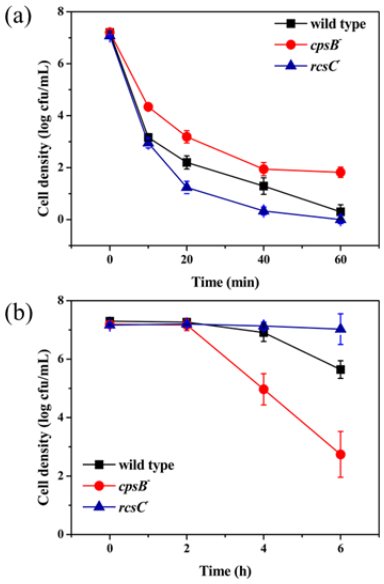

Figure 3

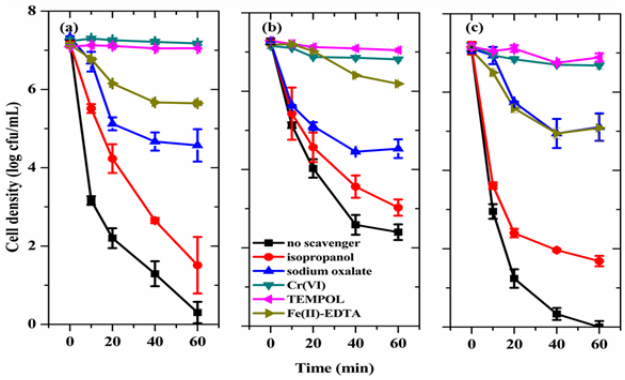

Figure 4

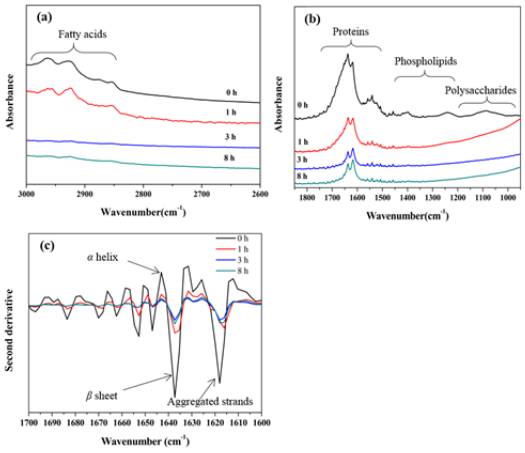

Figure 5

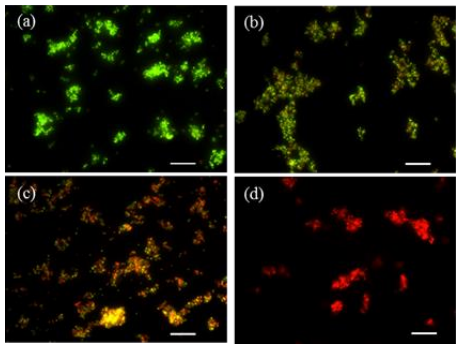

Figure 6

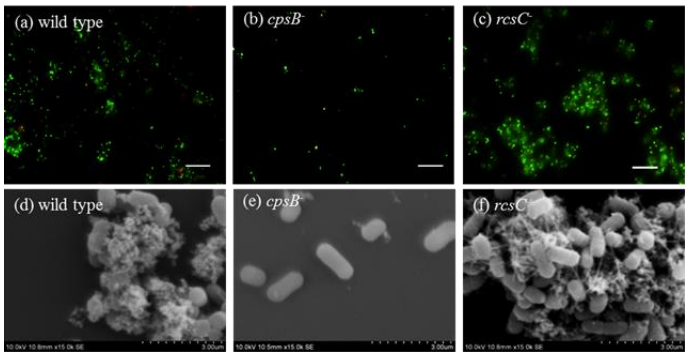

Figure 7

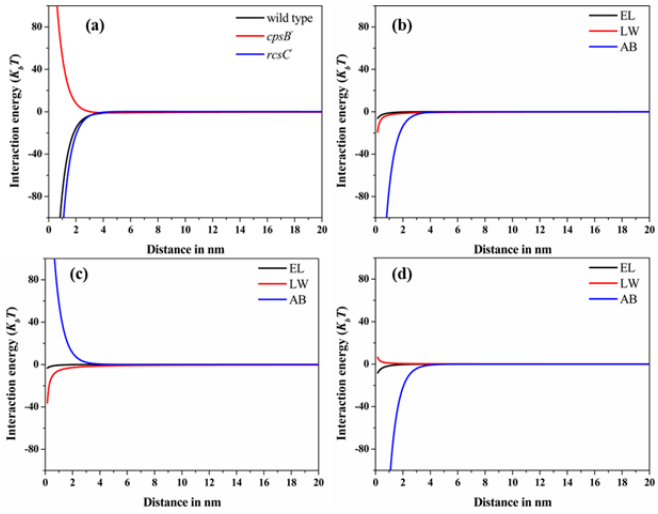

Table 1. Surface energy of TiO_2 and *E. coli* cells in mJ/m^{-2}

	γ_L^{LW}	γ_L^+	γ_L^-	γ_L^{AB}	$\Delta G_{d_0}^{AB}$	A in 10^{-21} J
TiO_2	5.5	47.5	32.2	29.8		
wild type	6.4	43.0	33.1	25.2	-2.3	-0.512
cpsB⁻ mutant	4.8	50.3	30.9	28.4	1.8	-0.979
rcsC⁻ mutant	9.3	42.3	39.7	20.7	-3.6	0.177